



RESEARCH LETTER

10.1029/2022GL098007

Key Points:

- Mars' magnetotail can be twisted up to 60 deg away from its expected location based on interplanetary magnetic field (IMF) draping, much greater than Earth's tail twist
- MAVEN observations show that Mars' tail exhibits larger twisting for $+B_Y$ IMF orientation, compared to $-B_Y$ IMF
- Mars crustal magnetic fields may play a significant role in shaping the twisted structure of the Martian magnetotail

Correspondence to:

G. A. DiBraccio,
gina.a.dibraccio@nasa.gov

Citation:

DiBraccio, G. A., Romanelli, N., Bowers, C. F., Gruesbeck, J. R., Halekas, J. S., Ruhunusiri, S., et al. (2022). A statistical investigation of factors influencing the magnetotail twist at Mars. *Geophysical Research Letters*, 49, e2022GL098007. <https://doi.org/10.1029/2022GL098007>

Received 21 JAN 2022
 Accepted 11 MAY 2022

Author Contributions:

Formal analysis: Gina A. DiBraccio
Investigation: Gina A. DiBraccio
Visualization: Gina A. DiBraccio
Writing – original draft: Gina A. DiBraccio
Writing – review & editing: Gina A. DiBraccio

© 2022. The Authors. This article has been contributed to by U.S. Government employees and their work is in the public domain in the USA.

This is an open access article under the terms of the [Creative Commons Attribution-NonCommercial-NoDerivs License](https://creativecommons.org/licenses/by-nc-nd/4.0/), which permits use and distribution in any medium, provided the original work is properly cited, the use is non-commercial and no modifications or adaptations are made.

A Statistical Investigation of Factors Influencing the Magnetotail Twist at Mars

Gina A. DiBraccio¹ , Norberto Romanelli^{1,2} , Charles F. Bowers³ , Jacob R. Gruesbeck¹ , Jasper S. Halekas⁴ , Suranga Ruhunusiri⁴ , Tristan Weber^{1,5}, Jared R. Easley¹ , Shaosui Xu⁶ , Janet G. Luhmann⁶ , Yuki Harada⁷ , Eduard Dubinin⁸ , Gang Kai Poh^{1,9} , David A. Brain¹⁰ , and Shannon M. Curry⁶ 

¹NASA Goddard Space Flight Center, Greenbelt, MD, USA, ²Department of Astronomy, University of Maryland, College Park, MD, USA, ³Department of Climate and Space Sciences and Engineering, University of Michigan, Ann Arbor, MI, USA, ⁴Department of Physics and Astronomy, The University of Iowa, Iowa City, IA, USA, ⁵Department of Physics and Astronomy, Howard University, Washington, DC, USA, ⁶Space Sciences Laboratory, University of California, Berkeley, CA, USA, ⁷Department of Geophysics, Graduate School of Science, Kyoto University, Kyoto, Japan, ⁸Max-Planck-Institute for Solar System Research, Göttingen, Germany, ⁹Catholic University of America, Washington, DC, USA, ¹⁰Laboratory for Atmospheric and Space Physics, University of Colorado, Boulder, CO, USA

Abstract The Martian magnetotail exhibits a highly twisted configuration, shifting in response to changes in polarity of the interplanetary magnetic field's (IMF) dawn-dusk (B_Y) component. Here, we analyze ~6000 MAVEN orbits to quantify the degree of magnetotail twisting (θ_{Twist}) and assess variations as a function of (a) strong planetary crustal field location, (b) Mars season, and (c) downtail distance. The results demonstrate that θ_{Twist} is larger for a duskward ($+B_Y$) IMF orientation a majority of the time. This preference is likely due to the local orientation of crustal magnetic fields across the surface of Mars, where a $+B_Y$ IMF orientation presents ideal conditions for magnetic reconnection to occur. Additionally, we observe an increase in θ_{Twist} with downtail distance, similar to Earth's magnetotail. These findings suggest that coupling between the IMF and moderate-to-weak crustal field regions may play a major role in determining the magnetospheric structure at Mars.

Plain Language Summary MAVEN magnetic field data are analyzed to understand factors that may influence the magnetotail structure at Mars. The Martian magnetotail lobes are observed to be twisted and the degree of this twist can vary. In this work, we calculate the degree of tail twist and monitor how it changes. To understand how the twist changes, we examine these variations as a function of Mars crustal field location, Mars season, and downtail distance away from Mars.

1. Introduction

The magnetic environment of Mars exhibits characteristics similar to both induced and intrinsic planetary magnetospheres. The elongated Martian magnetotail, created through the solar wind-planetary interaction, is comprised of a combination of planetary crustal magnetic fields (Acuña et al., 1998, 1999; Connerney et al., 2005) and the draped interplanetary magnetic field (IMF) (Crider et al., 2004; Romanelli et al., 2015; Yeroshenko et al., 1990). This unique amalgamation of crustal fields and IMF suggests that the Martian magnetotail structure and dynamics are likely distinct from that of induced magnetospheres (e.g., Venus) or intrinsic magnetospheres (e.g., Earth), but rather in a category of their own, as first suggested by Dubinin et al. (1980). Recent investigations of the Martian magnetotail have indicated just that – the tail is best described to be a hybrid regime exhibiting features and field topologies observed in both induced and intrinsic magnetospheres (DiBraccio et al., 2018; Dubinin et al., 2017; Luhmann et al., 2015).

The magnetotail of Mars experiences ubiquitous plasma features such as magnetic reconnection (Eastwood et al., 2008; Halekas et al., 2009; Harada et al., 2015, 2017; Ma et al., 2018) and reconnection-driven particle acceleration (Harada et al., 2020). Particles have also been observed to undergo acceleration due to magnetic shear stresses imposed by the draped IMF (Dubinin et al., 1993). Current sheets have been observed throughout the magnetotail (Artemyev et al., 2017; Grigorenko et al., 2019; Halekas et al., 2006), exhibiting flapping motions (DiBraccio et al., 2017) and quasi-adiabatic ion dynamics (Grigorenko et al., 2017). Magnetic flux ropes are common structures (Brain, Baker, et al., 2010; Briggs et al., 2011; DiBraccio et al., 2015; Eastwood et al., 2012; Hara et al., 2014, 2015) that may be formed either within the tail current sheet or in the ionosphere

(Bowers et al., 2021; Hara et al., 2017). The Martian magnetotail also serves as a major pathway for atmospheric escape (e.g., Brain, Barabash, et al. (2010); Dong et al. (2017); Dubinin et al. (2011, 2021); Halekas et al. (2016); Lundin (2011)).

Earlier investigations at Mars have explored the structure of the tail and predicted a deviation from the canonical depiction that includes only crustal fields and draped IMF (e.g., Brain et al. (2003); Luhmann et al. (2015); Ma et al. (2004); Mitchell et al. (2001)). Instead, it was suggested that the tail is comprised of three magnetic field topologies: (a) closed, with both ends attached to the planet; (b) open, with one end attached to the planet and the other connected to the solar wind; and (c) draped, with both ends in the solar wind. The open fields are a result of magnetic reconnection occurring between the draped IMF and closed crustal magnetic fields. Studies utilizing Mars Atmosphere and Volatile Evolution (MAVEN) magnetic field and electron measurements have confirmed these three field topologies and mapped their occurrence throughout the magnetosphere (Weber et al., 2017; Xu et al., 2016, 2019). Furthermore, the observed magnetic field topology within the tail has been reported to change as a function of solar wind pressure (Weber et al., 2019) and IMF direction (Xu et al., 2020) due to the occurrence of magnetic reconnection between the closed crustal fields and open fields draped around the planet (Weber et al., 2020).

Numerical simulations have played an essential role in interpreting the observations of Mars' complex magnetosphere. In addition to reproducing the average magnetotail field geometry (DiBraccio et al., 2018; Ulusen et al., 2016) and topology (Xu, Mitchell, Liemohn, et al., 2017; Xu, Mitchell, Luhmann, et al., 2017), time-dependent versions have been used to visualize how the observed dynamics are partly driven by planetary rotation, which constantly changes the crustal field orientation in the solar wind interaction, as well as the temporal variations in the external conditions (IMF and solar wind pressure) (Ma et al., 2015; Modolo et al., 2012; Romanelli et al., 2018).

The MAVEN data-model comparisons by DiBraccio et al. (2018) clearly revealed the IMF orientation-dependent twisted magnetotail configuration that supports the hybrid magnetosphere concept. This analysis utilized MAVEN data, along with magnetohydrodynamic simulations, and confirmed that the Martian magnetotail lobes exhibit a twist away from the nominal location expected from draped IMF alone. This twist was observed and modeled to change as a function of IMF B_y . DiBraccio et al. (2018) showed that the twist results from the contributions of open magnetic fields, suggesting that magnetic reconnection between the crustal fields and upstream IMF plays a role in driving the tail twist at Mars. However, the exact mechanism responsible for producing this Mars magnetotail twist remains to be established.

With additional in situ data available from the MAVEN spacecraft (Jakosky et al., 2015), it is now possible to perform a statistical study to assess factors in the Martian environment that may be contributing to the tail twist at Mars. In this study, we follow the data analysis methodologies implemented by DiBraccio et al. (2018) to examine the degree of magnetotail twisting at Mars as a function of (a) the location of the strong planetary crustal fields, (b) Mars season, and (c) downtail distance away from the planet. The implications of these findings contribute to our knowledge of the magnetotail structure, which impacts the ability of the Martian atmosphere to escape to space and enhances our understanding of sun-planetary interactions.

2. MAVEN Data and Methodology

This investigation utilizes five years of MAVEN magnetic field and plasma data from November 2014 through November 2019, presented in Mars solar orbital (MSO) coordinates: X_{MSO} is directed from the center of the planet to the center of the Sun, Z_{MSO} is perpendicular to the planet's orbital plane, and Y_{MSO} completes the right-handed system. MAVEN's Magnetometer (MAG) (Connerney et al., 2015) samples the local magnetic environment at Mars with a maximum rate of 32 vectors s^{-1} . The Solar Wind Ion Analyzer (SWIA) (Halekas et al., 2015) provides measurements of ion distributions over an energy range of 25 eV to 25 keV at cadences up to 4 s.

To select events for this study, we identify orbits with pristine in situ solar wind measurements using the algorithm developed by Halekas et al. (2017), which combines SWIA and MAG observations upstream of the bow shock (see description in Halekas et al. (2017) and implementation in DiBraccio et al. (2018)). The orbits resulting from this algorithmic survey provide a conservative collection of periods with stable IMF, as it omits periods of increased foreshock activity. Direct upstream measurements, however, are not always available due to

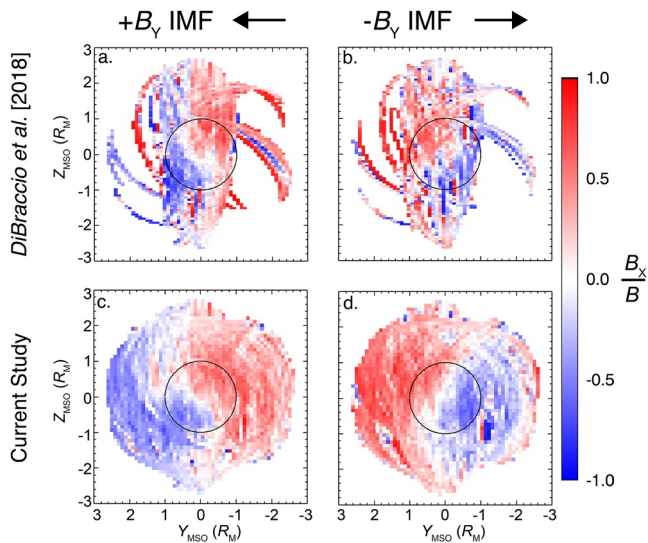


Figure 1. Magnetic maps of the normalized, average B_x component in the Martian magnetotail, separated $+B_y$ IMF (left column) and $-B_y$ IMF (right column) cases. The maps are projections in the $Y_{\text{MSO}}-Z_{\text{MSO}}$ plane, as viewed from the magnetotail looking towards Mars. Red sectors, $+B_x/B$, represent the sunward tail lobes, while blue sectors, $-B_x/B$, represent the antisunward tail lobes. The black circle represents Mars. (a) and (b) show the original results and coverage from DiBraccio et al. (2018), while (c) and (d) display the updated maps from this present study.

MAVEN's orbital precession. To augment the catalog of orbits, we employ the Ruhunusiri et al. (2018) method for inferring solar wind proxies during periods when in situ IMF observations were not available. This technique implements an artificial neural network to infer proxies of solar wind ion density, speed, and temperature, along with IMF direction and magnitude, from spacecraft measurements within the magnetosheath. The Ruhunusiri et al. (2018) solar wind proxies exhibit smaller uncertainties for IMF orientations with higher occurrence rates and has demonstrated that orientations with large statistics have uncertainties of 30° or less, which is more than sufficient for this investigation.

To accept an orbit for analysis in this study, we require that measurements of both the IMF, either in situ or by proxy, and the Martian magnetotail were available for a given orbit and utilize these observations from the same orbit. MAVEN's orbital period is ~ 4 hr, which implies that the time between IMF and magnetotail measurements is within $\sim 1-2$ hr. This timescale is within the period that Marquette et al. (2018) found the IMF cone and clock angles to be moderate-to-strongly autocorrelated, based on their analysis of MAVEN solar wind observations. Here, we define the tail as measurements occurring at a downtail distance of $X_{\text{MSO}} \leq -1 R_M$ (where R_M is the radius of Mars, or ~ 3997 km), which includes data from the nightside surface of Mars to the farthest downtail distances covered by MAVEN. There were no initial restrictions in the Y_{MSO} and Z_{MSO} directions for event selection; however, spatial constraints are later applied, as explained in Section 2.2. To characterize the orientation of magnetic fields within the magnetotail, 30-s averages are calculated from the full resolution MAG data.

By augmenting the data set with nearly two more years of MAVEN measurements, plus the new inclusion of solar wind proxies, we have accepted a total of 5940 orbits. This is more than four times the number of orbits analyzed in the original DiBraccio et al. (2018) investigation. Of these orbits, 2865 events ($\sim 48\%$) utilize direct IMF observations, while 3075 orbits ($\sim 52\%$) leverage IMF proxy information.

2.1. Statistical Analysis

The selected 5940 orbits are first analyzed using magnetic maps, which are created by normalizing B_x with respect to the local total field magnitude, B_x/B , and then averaging this normalized value over all orbits in $0.1 R_M \times 0.1 R_M$ bins (see description and implementation in DiBraccio et al. (2018)). These maps display the average, normalized B_x component of the magnetic field in the tail, projected into the $Y_{\text{MSO}}-Z_{\text{MSO}}$ plane. The IMF B_y component was observed to have the most significant influence on tail twisting patterns (DiBraccio et al., 2018), therefore, the magnetic maps are constructed as a function of IMF B_y polarity.

A comparison between magnetic maps from DiBraccio et al. (2018) and the orbits selected in this current investigation is displayed in Figure 1. The maps demonstrate improved coverage throughout the Martian magnetotail, thanks to the additional orbits. Both maps in Figures 1c and 1d contain more than 2500 orbits, with more than 200 orbits per bin, on average. Furthermore, the updated magnetic maps in Figures 1c and 1d continue to display the twisted tail configuration, changing as a function of IMF B_y direction. With respect to the X_{MSO} axis, the tail lobes are twisted in the counterclockwise and clockwise directions from their nominal draping pattern for $+B_y$ and $-B_y$ IMF, respectively.

2.2. Quantifying the Tail Twist

To assess changes in the Martian tail twist, we establish a technique for quantifying the degree of tail twisting. The first step in evaluating the angle at which the tail lobes have twisted away from their expected nominal draping pattern, θ_{Twist} , is to determine the center of each lobe on a magnetic map. This is done by calculating the center of the area composed of red bins ($+B_x/B$) and blue bins ($-B_x/B$) for the sunward and antisunward lobes, respectively (green dots in Figures 2a and 2b). The centers are determined by computing the geometric centroid

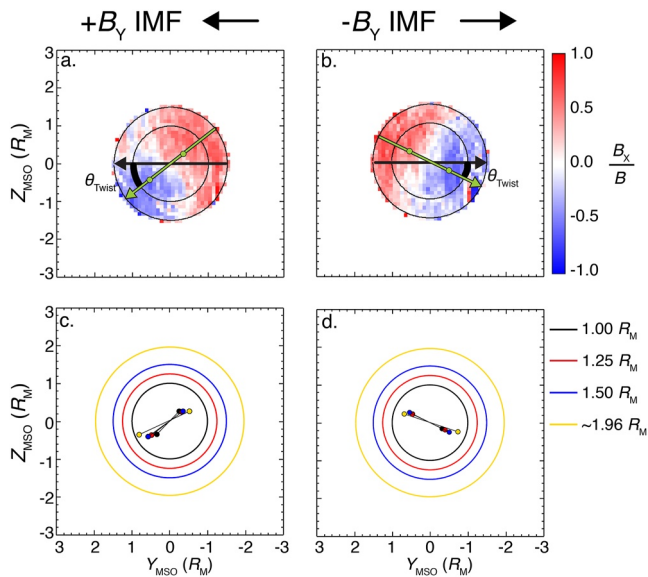


Figure 2. An example of magnetic maps generated with a $1.50-R_M$ radius spatial constraint (outer black circle) for (a) $+B_Y$ and (b) $-B_Y$ IMF. Green dots represent the centers of each lobe. The lobe vector (green vector) identifies the actual tail lobe location compared with the expected draped lobe location based on IMF draping (black vector). θ_{Twist} is highlighted as the thick black arc between the vectors. Colored concentric circles and dots represent the spatial constraints and resulting lobe centers, respectively, that were tested for (c) $+B_Y$ and (d) $-B_Y$ IMF using radii of $1.00 R_M$ (black), $1.25 R_M$ (red), $1.50 R_M$ (blue), and $\sim 1.96 R_M$ (yellow).

of the red/blue regions where each bin is assigned the same weight to focus on the spatial extent of the lobes rather than areas of intensity. Note that the determination of the lobe centers relies on the large statistics and is therefore not based on the tail current sheet location. Next, we determine the lobe vector between these two centers, identified by the green arrow in Figures 2a and 2b. The lobe vector's initial and terminal points are defined as the center of the sunward ($+B_X/B$) and antisunward ($-B_X/B$) lobes, respectively. This vector is roughly perpendicular to the average current sheet location, indicated by the white region separating the two lobes in the magnetic maps. If no tail twisting is observed, the green lobe vector would align with the black IMF vector, which is the expected lobe location based on draped IMF following the Parker spiral model (Parker, 1958). Specifically, θ_{Twist} is defined as the angle between the observed lobe vector (green arrow) and the expected draped lobe vector (black arrow) as illustrated in Figure 2.

The twist angle is dependent on the spatial extent of the tail lobes in the $Y_{\text{MSO}}-Z_{\text{MSO}}$ plane. Because the data set selected in this study includes all measurements in the magnetotail when IMF information was available, it inevitably incorporates measurements outside of the tail lobes within the downtail magnetosheath. Therefore, we omit the magnetosheath data and examine how θ_{Twist} changes when implementing various spatial restrictions to define the tail lobes. To do this, we calculate θ_{Twist} over four spatial constraints in the $Y_{\text{MSO}}-Z_{\text{MSO}}$ plane. These are displayed as concentric circles in Figures 2c and 2d and defined as follows: (a) $1.00-R_M$ radius (i.e., the optical wake); (b) $1.25-R_M$ radius; (c) $1.50-R_M$ radius and (d) a $\sim 1.96-R_M$ radius, which is the nominal location of the induced magnetopause boundary (IMB) at a downtail distance of $X_{\text{MSO}} = -1.50 R_M$ (Vignes et al., 2000).

A comparison of the lobe centers based on the four concentric regimes in Figures 2c and 2d demonstrate minimal variability in θ_{Twist} . Therefore, we choose to implement the spatial restriction of $1.50-R_M$ radius in the $Y_{\text{MSO}}-Z_{\text{MSO}}$ plane (blue circle, Figures 2c and 2d) for the remainder of the analysis. This selection ensures that sufficient data are included, while applying a more conservative restriction than the radius based on the average IMB location, which could include magnetosheath IMF during periods of magnetospheric compression. Finally, to ensure adequate coverage, we set a requirement that $\geq 85\%$ of the bins within this $1.50-R_M$ radius must include data to accept a given magnetic map in this study. This requirement was also tested using thresholds of 80% and 90% coverage. The overall results did not vary significantly when changing this threshold, however, we made the decision to require 85% coverage to stay conservative while avoiding unnecessary data gaps introduced by the more extreme limit of 90% coverage.

To summarize the steps in this analysis, the following procedure is applied beyond the original analysis of DiBraccio et al. (2018) to calculate θ_{Twist} and further assess the factors influencing the tail twist at Mars as a function of $\pm B_Y$ IMF:

1. Implement a spatial constraint using a radius of $1.50 R_M$ in the $Y_{\text{MSO}}-Z_{\text{MSO}}$ plane to generate magnetic maps and analyze data within the magnetotail.
2. Only accept magnetic maps with data coverage in $\geq 85\%$ of the bins, omitting any maps with less coverage.
3. Calculate the lobe centers of the observed $\pm B_X$ tail lobes and define the lobe vector described by these centers (green vectors in Figures 2a and 2b).
4. Define the expected draped lobe vector based on typical IMF B_Y conditions (black vectors in Figures 2a and 2b).
5. Evaluate the degree of tail twist for a given magnetic map by calculating the angle, θ_{Twist} , between the observed and predicted lobe vectors.

Following these five steps, the magnetic maps and resulting θ_{Twist} values are able to be statistically analyzed. Variances in θ_{Twist} values would result from utilizing an alternative method for calculating the lobe centers or implementing different restrictions for spatial constraints and data coverage.

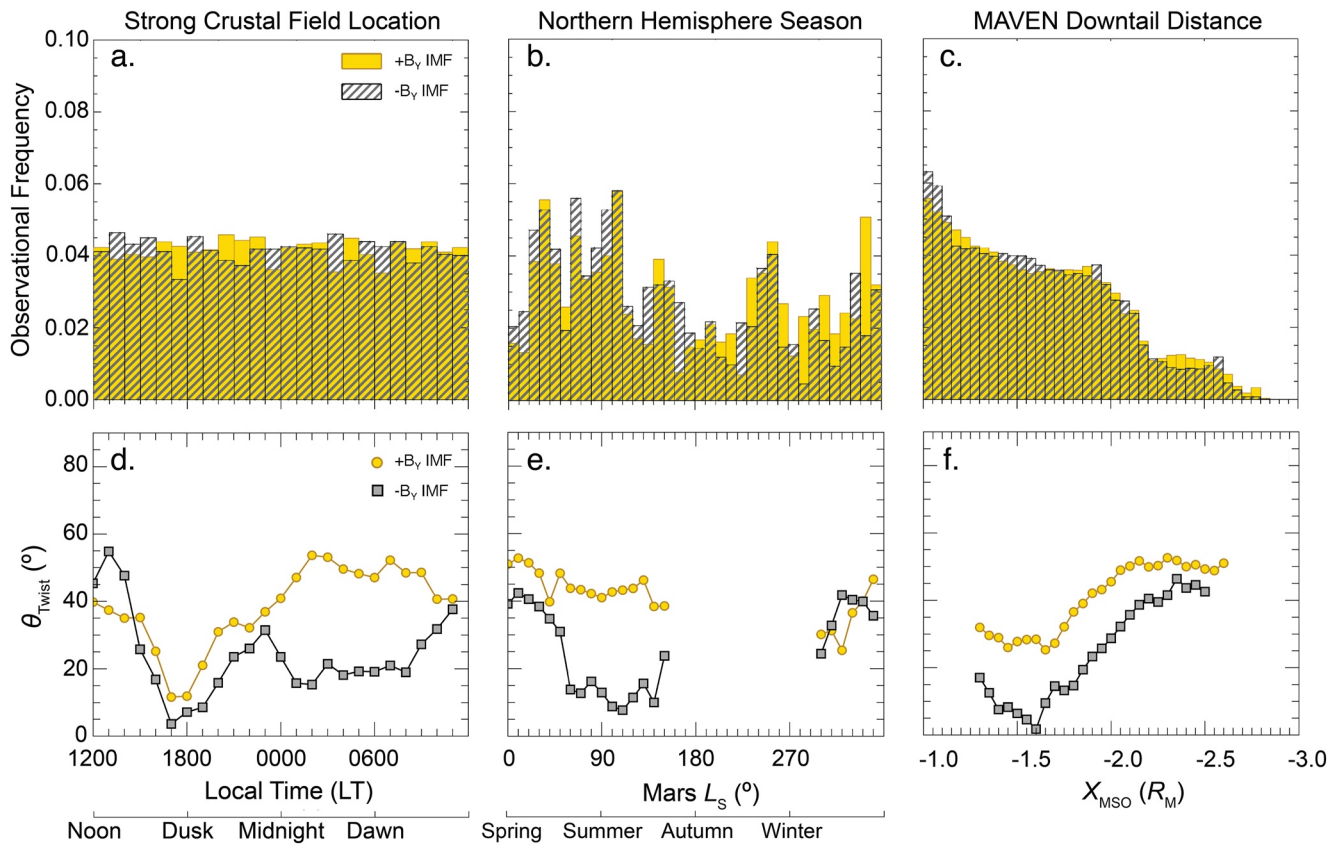


Figure 3. Histograms demonstrating the sampling frequency of the MAVEN orbits included in this study based on (a) strong crustal field location, (b) northern hemisphere season, and (c) downtail distance for $+B_Y$ (yellow) and $-B_Y$ (gray stripe) IMF. Scatterplots reveal changes in calculated θ_{Twist} values as a function of (d) strong crustal field location, (e) northern hemisphere season, and (f) downtail distance for $+B_Y$ (yellow circles) and $-B_Y$ (gray squares) IMF.

3. Results: Magnetotail Twist Dependencies

Magnetic maps are generated to assess the level of Mars tail twisting as a function of (a) strong crustal field location, (b) Mars season, and (c) downtail distance from the planet. For each of these three parameters, we study variations in the tail twist by repeatedly calculating θ_{Twist} using a sliding interval to advance through the entire parameter space, as described in detail below.

3.1. Dependency on Crustal Field Location

In this study, the influence of the Martian crustal fields is determined by the location of the strongest sources, denoted at 180°E longitude, in local time (LT) when MAVEN reached its furthest downtail distance along the X_{MSO} axis for a given orbit. The histograms in Figure 3a demonstrate the crustal field LT sampling frequency included in this investigation.

Individual magnetic maps are created over 4-h intervals in LT with a sliding window over 1-h increments to provide complete coverage of the full 24-h period. This analysis generates a total of 24 maps and corresponding θ_{Twist} calculations for both $+B_Y$ and $-B_Y$ IMF. The resulting θ_{Twist} values are displayed in Figure 3d where the points on the scatterplot are located at the midpoint of the interval used to calculate θ_{Twist} .

This analysis reveals that when the strong crustal fields are located on the dayside, close to noon (1200 LT), a peak in tail twisting is observed for a $-B_Y$ IMF orientation. When strong crustal fields are in the post-noon, pre-midnight sector, similar trends are observed in $+B_Y$ and $-B_Y$ IMF. These trends include a decrease in θ_{Twist} from day to dusk (1200–1800 LT), reaching a local minimum of $<15^\circ$ at dusk, followed by an increase between dusk to midnight (1800–2400 UT). In the post-midnight, pre-noon sector, the trends between $+B_Y$ and $-B_Y$ IMF

diverge. Results indicate that the tail twist remains larger for $+B_Y$ IMF, with values between 40 and 60°, while $-B_Y$ IMF shows a comparative decrease in θ_{Twist} as it remains $<40^\circ$.

3.2. Dependency on Mars Season

Seasonal variations in magnetotail twisting are determined by calculating θ_{Twist} as a function of Martian solar longitude (L_S). Here, L_S values are determined on an orbit-by-orbit basis. The sampling frequency of MAVEN orbits included in this study (Figure 3b) demonstrates a higher coverage between $L_S \sim 0\text{--}180^\circ$, encompassing northern spring and northern summer; however, coverage between IMF orientations is comparable.

Impacts of Mars season are studied by generating magnetic maps over L_S intervals of 90° with a 10° sliding window for complete coverage over the Martian year ($L_S \sim 0\text{--}360^\circ$). This results in a total of 36 magnetic maps, and corresponding θ_{Twist} calculations, for both $+B_Y$ and $-B_Y$ IMF. The variations in tail twist as a function of L_S are displayed in Figure 3e for $\pm B_Y$ IMF. Gaps are evident for $L_S \sim 160\text{--}290^\circ$ because the magnetic maps did not meet the 85% bin coverage criterion, likely due to decreased coverage displayed in Figure 3b.

The results demonstrate that from northern spring through northern autumn ($L_S \sim 0\text{--}160^\circ$), θ_{Twist} is greater for $+B_Y$ IMF. The $+B_Y$ IMF values remain between 40 and 55° while $-B_Y$ IMF calculations are $<45^\circ$ with more than half at $<20^\circ$. Additionally, θ_{Twist} is relatively constant for $+B_Y$ IMF during this interval while $-B_Y$ IMF experiences a significant decrease around northern summer. With limited information between northern autumn and northern winter ($L_S \sim 180\text{--}360^\circ$), Figure 3e suggests that the two curves may converge; however, additional data are needed to definitively determine this. Following the gap, both $\pm B_Y$ IMF orientations present an increase in θ_{Twist} between northern winter and northern spring ($L_S \sim 300\text{--}360^\circ$).

3.3. Dependency on Downtail Distance

To examine the Martian magnetotail twist as a function of downtail distance, we assess changes in θ_{Twist} between X_{MSO} values of $-1.00 R_M$ to $-2.81 R_M$, the latter being the furthest distance sampled by MAVEN in this study. The sampling frequency along X_{MSO} (Figure 3c) has a modestly higher rate closer to the planet that remains relatively steady before decreasing at distances $\leq -2.00 R_M$. This drop off at further downtail distances is expected due to MAVEN's orbital precession, which naturally offers greater coverage closer to the planet. The orbits included here provide comparable downtail coverage for both IMF configurations.

To determine whether the degree of tail twist changes as a function of distance from the Mars, magnetic maps are created from $0.6 R_M$ thick slices in the $Y_{\text{MSO}}\text{--}Z_{\text{MSO}}$ along the X_{MSO} axis. Using a sliding window interval of $0.05 R_M$, complete coverage is achieved over the $-1.00 R_M \geq X_{\text{MSO}} \geq -2.81 R_M$ range. This results in a total of 36 magnetic maps, and corresponding θ_{Twist} calculations, for both $+B_Y$ and $-B_Y$ IMF. Data gaps are present in Figure 3f for $X_{\text{MSO}} \leq -2.65 R_M$ in the $+B_Y$ IMF case and $X_{\text{MSO}} \leq -2.55 R_M$ for the $-B_Y$ IMF case due to decreased coverage (Figure 3c), causing the magnetic maps coverage to miss the 85% bin requirement.

The results demonstrate similar trends in θ_{Twist} as a function of downtail distance for both IMF configurations; however, the $+B_Y$ IMF orientation experiences larger θ_{Twist} values. In both cases, θ_{Twist} initially decreases and then steadily increases with distance from Mars between $X_{\text{MSO}} \sim -1.60 R_M$ to $\sim -2.40 R_M$. The initial decrease may be due to the influence of the closed crustal magnetic fields in this region close to the planet. The subsequent increase occurs at similar rates for $\pm B_Y$ IMF, but θ_{Twist} increases from 25° to 55° for $+B_Y$ IMF while the $-B_Y$ IMF case rises from $<5^\circ$ to 45° . The increasing trend in θ_{Twist} tapers off for both IMF directions near $X_{\text{MSO}} \sim -2.50 R_M$, which could be due to the lower frequency of MAVEN orbits further downtail.

4. Discussion

Motivated by the initial investigation of the Martian magnetotail twist by DiBraccio et al. (2018), we present statistical results to explore dependencies of this tail twist using an augmented MAVEN data set. The results provide further insight to the processes driving magnetospheric dynamics at Mars, influencing the twisted tail. Each of the three factors explored in Section 3 have been examined individually, although the tail twist is likely influenced by a combination of these parameters. The interplay between these three parameters and their effect on Mars' tail twist may be explored in the future as increased statistics allow.

The analysis based on crustal field location and variation in the twisting angles presented in Figure 3d demonstrates that the IMF-crustal field interaction plays a role in the degree of tail twisting and that we must consider changes in geometry of the local planetary crustal magnetic field vectors as they rotate. Magnetic reconnection is likely to occur when a large shear is present between the IMF and crustal fields, allowing the fields to couple and change topology. It is also possible for component magnetic reconnection to occur when a low shear between the IMF and crustal fields exists, but this may happen less frequently and generally requires a nearly equivalent field strength on either side of the reconnection region (Sonnerup, 1974).

The observed peak in θ_{Twist} when the strongest crustal fields were located at ~ 1200 LT (Figure 3d) suggests a preference for reconnection to occur for a $-B_Y$ -oriented IMF, likely due to the orientation of the underlying strong crustal fields. However, when these strong crustal fields are in the post-midnight sector (0000–0600 LT), larger values in θ_{Twist} for a $+B_Y$ -oriented IMF implies that the orientation of the moderate-to-weak crustal sources on the dayside favor this IMF configuration for reconnection to occur. Overall, these changes in θ_{Twist} as a function of strong crustal field location suggest that varying crustal field geometries and orientations across the surface of Mars changes the preferred dayside IMF orientation for magnetic reconnection to occur and θ_{Twist} to increase. The crustal field orientations away from the strong field region are more likely to reconnect with a $+B_Y$ IMF, while the orientation of the strong crustal fields is less likely.

A preference for $+B_Y$ IMF orientation in generating larger θ_{Twist} values is also observed in the results based on seasonal effects (Figure 3e) and downtail distance (Figure 3f). Significantly larger degrees of tail twist are observed for $+B_Y$ IMF, compared to $-B_Y$ IMF, during northern summer when the northern hemisphere directly interacts with the solar wind and the strong crustal fields are tilted away from the subsolar point. This trend suggests that the solar wind-Mars interaction may be heavily influenced by the interplay with the moderate-to-weak crustal fields and $+B_Y$ IMF. Future studies investigating trends of crustal field-IMF dayside interactions are needed to confirm this preference for IMF direction and influence on the overall magnetosphere structure.

As an alternative to the theory that solar wind-crustal field interactions are responsible for generating the magnetotail twist at Mars, Ramstad et al. (2020) mapped the global current system of the Martian magnetosphere and identified asymmetric sunward currents, unrelated to the crustal fields. If this current system is responsible for generating Mars's tail twist, then it would also be observed at Venus. In fact, Dubinin et al. (2014a) and Dubinin et al. (2014b) observed a difference in magnetic structures within the ionospheres of Venus and Mars, respectively, based on the direction of IMF B_Y . Both studies concluded that collisional effects decoupling ion and electron motion in the ionosphere are responsible for introducing hemispherical asymmetries in electric currents that change as a function of IMF direction. Asymmetries were also observed in the magnetosheath flow (Dubinin et al., 2018; Romanelli et al., 2020) and in the IMF draping pattern around Mars (Brain et al., 2006; Romanelli et al., 2015). The latter was determined to be a result of field lines wrapping around Mars and propagating based on the direction of the solar wind motional electric field (Dubinin et al., 2019). Although these asymmetries are present at Venus and Mars, the interplay between the draped IMF, current system structure, and magnetic reconnection must be considered to determine whether this tail twist is driven more by induced- or intrinsic-magnetosphere dynamics.

At Earth, extensive studies have been performed over the last four decades to investigate the cause of magnetotail twisting (e.g., Cowley (1981); Kaymaz et al. (1994); Khurana et al. (1996); Sibeck et al. (1985); Tenfjord et al. (2015); Xiao et al. (2016)). Statistics have determined that Earth's tail twist has typical values $<10^\circ$ (see Table 2 in Kaymaz et al. (1994)), which is much smaller than the values reported here for Mars. Furthermore, several investigations have revealed that the Earth's magnetotail exhibits a larger degree of tail twisting under $+B_Y$ IMF conditions (Kaymaz et al., 1994; Owen et al., 1995; Pitkänen et al., 2021), similar to the trends observed at Mars. While many theories exist to explain the magnetotail twist at Earth, the exact cause remains to be proven. A theory by Cowley (1981), suggests that dayside magnetic reconnection generates open field lines that exert a torque on the magnetotail lobes and rotate the current sheet. Tenfjord et al. (2015) considers that magnetic flux may be asymmetrically added to the tail lobes, resulting from patterns of reconnection located on the dayside magnetopause.

The similarities that have been observed between Mars and both Earth and Venus, demonstrates that further analyses are needed to understand which mechanisms and dynamics are generating the magnetotail twist. That is, we must explore whether intrinsic magnetosphere processes (i.e., dayside reconnection) versus induced

magnetosphere mechanisms (i.e., IMF draping and asymmetric current systems) play a larger role in the hybrid magnetosphere of Mars. Future investigations will utilize data available at Mercury and Venus to further explore whether magnetotail twisting is present at other intrinsic and induced magnetospheres to better understand the processes responsible for shaping the structure and dynamics of the Mars space environment.

Data Availability Statement

MAVEN data are publicly available through the Planetary Plasma Interactions Node of the Planetary Data System (<https://pds-ppi.igpp.ucla.edu/mission/MAVEN/MAVEN/MAG>).

Acknowledgments

The MAVEN project is supported by NASA through the Mars Exploration Program. N.R. and G.P. are supported through a cooperative agreement with Center for Research and Exploration in Space Sciences & Technology II (CRESST II) between NASA Goddard Space Flight Center and University of Maryland College Park under award number 80GSFC21M0002. E.D. wishes to acknowledge support from DFG grants TE 664/4-1 and PA 525/25-1.

References

- Acuña, M. H., Connerney, J. E. P., Ness, Lin, R. P., Mitchell, D., Carlson, C. W., et al. (1999). Global distribution of crustal magnetization discovered by the Mars Global Surveyor MAG/ER experiment. *Science*, *284*, 790–793. <https://doi.org/10.1126/science.284.5415.790>
- Acuña, M. H., Connerney, J. E. P., Wasilewski, P. A., Lin, R. P., Anderson, K. A., Carlson, C. W., et al. (1998). Magnetic field and plasma observations at Mars: Initial results of the Mars global surveyor mission. *Science*, *279*(5357), 1676–1680.
- Artemyev, A. V., Angelopoulos, V., Halekas, J. S., Runov, A., Zelenyi, L. M., & McFadden, J. P. (2017). Mars's magnetotail: Nature's current sheet laboratory. *Journal of Geophysical Research: Space Physics*, *122*, 5404–5417. <https://doi.org/10.1002/2017JA024078>
- Bowers, C. F., Slavin, J. A., DiBraccio, G. A., Poh, G., Hara, T., Xu, S., & Brain, D. A. (2021). MAVEN survey of magnetic flux rope properties in the Martian ionosphere: Comparison with three types of formation mechanisms. *Geophysical Research Letters*, *48*. <https://doi.org/10.1029/2021GL093296>
- Brain, D., Barabash, S., Boesswetter, A., Bougher, S., Brecht, S., Chanteur, G., et al. (2010). A comparison of global models for the solar wind interaction with Mars. *Icarus*, *206*, 139–151. <https://doi.org/10.1016/j.icarus.2009.06.030>
- Brain, D. A., Bagenal, F., Acuna, M. H., & Connerney, J. E. P. (2003). Martian magnetic morphology: Contributions from the solar wind and crust. *Journal of Geophysical Research*, *108*. <https://doi.org/10.1029/2002JA009482>
- Brain, D. A., Baker, A. H., Briggs, J., Eastwood, J. P., Halekas, J. S., & Phan, T. D. (2010). Episodic detachment of Martian crustal magnetic fields leading to bulk atmospheric plasma escape. *Geophysical Research Letters*, *37*. <https://doi.org/10.1029/2010GL043916>
- Brain, D. A., Mitchell, D., & Halekas, J. (2006). *The magnetic eld draping direction at Mars from April 1999 through August 2004*. <https://doi.org/10.1016/icarus.2005.09.023>
- Briggs, J. A., Brain, D. A., Cartwright, M. L., Eastwood, J. P., & Halekas, J. S. (2011). A statistical study of flux ropes in the Martian magnetosphere. *Planetary and Space Science*, *59*, 1498–1505. <https://doi.org/10.1016/j.pss.2011.06.010>
- Connerney, J. E. P., Acuna, M. H., Ness, N. F., Kletetschka, G., Mitchell, D. L., Lin, R. P., & Reme, H. (2005). Tectonic implications of Mars crustal magnetism. *P Natl Acad Sci USA*, *102*(42), 14970–14975. <https://doi.org/10.1073/pnas.0507469102>
- Connerney, J. E. P., Espley, J., Lawton, P., Murphy, S., Odom, J., Oliverson, R., & Sheppard, D. (2015). The MAVEN Magnetic Field Investigation. *Space Science Reviews*, *195*(1–4), 257–291. <https://doi.org/10.1007/s11214-015-0169-4>
- Cowley, S. W. H. (1981). Magnetospheric asymmetries associated with the Y-component of the IMF. *Planetary and Space Science*, *29*, 79–96. [https://doi.org/10.1016/0032-0633\(81\)90141-0](https://doi.org/10.1016/0032-0633(81)90141-0)
- Crider, D. H., Brain, D. A., Acuna, M. H., Vignes, D., Mazelle, C., & Bertucci, C. (2004). Mars Global Surveyor observations of solar wind magnetic field draping around Mars. *Space Science Reviews*, *111*(1–2), 203–221. https://doi.org/10.1007/978-0-306-48604-3_5
- DiBraccio, G. A., Dann, J., Espley, J. R., Gruesbeck, J. R., Soobiah, Y., Connerney, J. E. P., et al. (2017). MAVEN observations of tail current sheet flapping at Mars. *Journal of Geophysical Research: Space Physics*, *122*, 4308–4324. <https://doi.org/10.1002/2016JA023488>
- DiBraccio, G. A., Espley, J. R., Gruesbeck, J. R., Connerney, J. E. P., Brain, D. A., Halekas, J. S., et al. (2015). Magnetotail dynamics at Mars: Initial MAVEN observations. *Geophysical Research Letters*, *42*, 8828–8837. <https://doi.org/10.1002/2015GL065248>
- DiBraccio, G. A., Luhmann, J. G., Curry, S. M., Espley, J. R., Xu, S., Mitchell, D. L., et al. (2018). The twisted configuration of the Martian magnetotail: MAVEN observations. *Geophysical Research Letters*, *45*, 4559–4568. <https://doi.org/10.1029/2018GL077251>
- Dong, Y., Fang, X., Brain, D. A., McFadden, J. P., Halekas, J. S., Connerney, J. E. P., et al. (2017). Seasonal variability of Martian ion escape through the plume and tail from MAVEN observations. *Journal of Geophysical Research: Space Physics*, *122*, 4009–4022. <https://doi.org/10.1002/2016JA023517>
- Dubinin, E., Fraenz, M., Fedorov, A., Lundin, R., Edberg, N., Duru, F., & Vaisberg, O. (2011). Ion energization and escape on Mars and Venus. *Space Science Reviews*, 173–211. https://doi.org/10.1007/978-1-4614-3290-6_6
- Dubinin, E., Fraenz, M., Pätzold, M., Halekas, J. S., McFadden, J., Connerney, J. E. P., et al. (2018). Solar wind deflection by mass loading in the Martian magnetosheath based on MAVEN observations. *Geophysical Research Letters*, *45*, 2574–2579. <https://doi.org/10.1002/2017GL076813>
- Dubinin, E., Fraenz, M., Pätzold, M., McFadden, J., Halekas, J. S., DiBraccio, G. A., et al. (2017). The effect of solar wind variations on the escape of oxygen ions from Mars through diurnal channels: MAVEN observations. *Journal of Geophysical Research: Space Physics*, *122*. <https://doi.org/10.1002/2017JA024741>
- Dubinin, E., Fraenz, M., Pätzold, M., Tellmann, S., Woch, J., McFadden, J., & Zelenyi, L. (2021). Bursty ion escape fluxes at Mars. *Journal of Geophysical Research: Space Physics*, *126*. <https://doi.org/10.1029/2020JA028920>
- Dubinin, E., Fraenz, M., Zhang, T. L., Woch, J., & Wei, Y. (2014b). Magnetic elds in the Mars ionosphere of a noncrustal origin: Magnetization features. *Geophysical Research Letters*, *41*, 6329–6334. <https://doi.org/10.1002/2014GL061453>
- Dubinin, E., Fraenz, M., Zhang, T. L., Woch, J., & Wei, Y. (2014a). Magnetic elds in the Venus ionosphere: Dependence on the IMF direction: Venus express observations. *Journal of Geophysical Research: Space Physics*, *119*, 7587–7600. <https://doi.org/10.1002/2014JA020195>
- Dubinin, E., Israelevich, P. L., & Podgomy, I. M. (1980). Combined magnetosphere. *Cosmic Research*, *18*(470). [https://doi.org/10.1016/0008-6223\(80\)90007-x](https://doi.org/10.1016/0008-6223(80)90007-x)
- Dubinin, E., Lundin, R., Norberg, O., & Pissarenko, N. (1993). Ion-Acceleration in the Martian Tail: Phobos Observations. *Journal of Geophysical Research: Space Physics*. <https://doi.org/10.1029/92JA02233>
- Dubinin, E., Modolo, R., Fraenz, M., Pätzold, M., Woch, J., Chai, L., et al. (2019). The induced magnetosphere of Mars: Asymmetrical topology of the magnetic field lines. *Geophysical Research Letters*, *46*, 12722–12730. <https://doi.org/10.1029/2019GL084387>

- Eastwood, J. P., Brain, D. A., Halekas, J. S., Drake, J. F., & Phan, T. D., (2008). Evidence for collisionless magnetic reconnection at Mars. *Geophysical Research Letters*, 35. <https://doi.org/10.1029/2007GL032289>
- Eastwood, J. P., Videira, J. J. H., Brain, D. A., & Halekas, J. S. (2012). A chain of magnetic flux ropes in the magnetotail of Mars. *Geophysical Research Letters*, 39. <https://doi.org/10.1029/2011GL050444>
- Grigorenko, E. E., Shuvalov, S. D., Malova, H. V., Dubinin, E., Popov, V. Y., Zelenyi, L. M., et al. (2017). Imprints of quasi-adiabatic ion dynamics on the current sheet structures observed in the Martian magnetotail by MAVEN. *Journal of Geophysical Research: Space Physics*, 122, 176–180. <https://doi.org/10.1002/2017JA024216>
- Grigorenko, E. E., Zelenyi, L. M., DiBraccio, G. A., Ermakov, V. N., Shuvalov, S. D., Malova, H. V., et al. (2019). Thin current sheets of sub-ion scales observed by MAVEN in the Martian magnetotail. *Geophysical Research Letters*, 46, 6214–6222. <https://doi.org/10.1029/2019GL082709>
- Halekas, J. S., Brain, D. A., Lillis, R. J., Fillingim, M. O., Mitchell, D. L., & Lin, R. P. (2006). Current sheets at low altitudes in the Martian magnetotail. *Geophysical Research Letters*, 33. <https://doi.org/10.1029/2006GL026229>
- Halekas, J. S., Brain, D. A., Ruhunusiri, S., McFadden, J. P., Mitchell, D. L., Mazelle, C., et al. (2016). Plasma clouds and snowplows: Bulk plasma escape from Mars observed by MAVEN. *Geophysical Research Letters*, 43, 1426–1434. <https://doi.org/10.1002/2016GL067752>
- Halekas, J. S., Eastwood, J. P., Brain, D. A., Phan, T. D., Oieroset, M., & Lin, R. P. (2009). In situ observations of reconnection Hall magnetic fields at Mars: Evidence for ion diffusion region encounters. *Journal of Geophysical Research: Space Physics*, 114. <https://doi.org/10.1029/2009JA014544>
- Halekas, J. S., Ruhunusiri, S., Harada, Y., Collinson, G., Mitchell, D. L., Mazelle, C., et al. (2017). Structure, dynamics, and seasonal variability of the Mars-solar wind interaction: MAVEN Solar Wind Ion Analyzer in-flight performance and science results. *Journal of Geophysical Research: Space Physics*, 122, 547–578. <https://doi.org/10.1002/2016JA023167>
- Halekas, J. S., Taylor, E. R., Dalton, G., Johnson, G., Curtis, D. W., McFadden, J. P., et al. (2015). The Solar Wind Ion Analyzer for MAVEN. *Space Science Reviews*. <https://doi.org/10.1007/s11214-013-0029-z>
- Hara, T., Harada, Y., Mitchell, D. L., DiBraccio, G. A., Espley, J. R., Brain, D. A., et al. (2017). On the origins of magnetic flux ropes in near-Mars magnetotail current sheets. *Geophysical Research Letters*, 44, 7653–7662. <https://doi.org/10.1002/2017gl073754>
- Hara, T., Mitchell, D. L., McFadden, J. P., Seki, K., Brain, D. A., Halekas, J. S., et al. (2015). Estimation of the spatial structure of a detached magnetic flux rope at Mars based on simultaneous MAVEN plasma and magnetic field observations. *Geophysical Research Letters*, 42, 8933–8941. <https://doi.org/10.1002/2015GL065720>
- Hara, T., Seki, K., Hasegawa, H., Brain, D. A., Matsunaga, K., Saito, M. H., & Shiota, D. (2014). Formation processes of flux ropes downstream from Martian crustal magnetic fields inferred from Grad-Shafranov reconstruction. *Journal of Geophysical Research: Space Physics*, 119, 7947–7962. <https://doi.org/10.1002/2014JA019943>
- Harada, Y., Halekas, J. S., McFadden, J. P., Espley, J., DiBraccio, G. A., Mitchell, D. L., et al. (2017). Survey of magnetic reconnection signatures in the Martian magnetotail with MAVEN. *Journal of Geophysical Research: Space Physics*, 122, 5114–5131. <https://doi.org/10.1002/2017ja023952>
- Harada, Y., Halekas, J. S., McFadden, J. P., Mitchell, D. L., Mazelle, C., Connerney, J. E. P., et al. (2015). Magnetic reconnection in the near-Mars magnetotail: MAVEN observations. *Geophysical Research Letters*, 42(21), 8838–8845. <https://doi.org/10.1002/2015gl065004>
- Harada, Y., Halekas, J. S., Xu, S., DiBraccio, G. A., Ruhunusiri, S., Hara, T., et al. (2020). Ion jets within current sheets in the Martian magnetosphere. *Journal of Geophysical Research: Space Physics*, 125. <https://doi.org/10.1029/2020JA028576>
- Jakosky, B. M., Lin, R. P., Grebowsky, J. M., Luhmann, J. G., Mitchell, D. F., Beutelschies, G., et al. (2015). The Mars atmosphere and volatile evolution (MAVEN) mission. *Space Science Reviews*, 195, 3–48. <https://doi.org/10.1007/s11214-015-0139-x>
- Kaymaz, Z., Siscoe, G. L., Luhmann, J. G., Lepping, R. P., & Russell, C. T. (1994). Interplanetary magnetic-field control of magnetotail magnetic-field geometry: Imp-8 observations. *Journal of Geophysical Research: Space Physics*, 99, 11113. <https://doi.org/10.1029/94JA00300>
- Khurana, K. K., Walker, R. J., & Ogino, T. (1996). Magnetospheric convection in the presence of interplanetary magnetic field By: A conceptual model and simulations. *Journal of Geophysical Research*, 101, 4907–4916. <https://doi.org/10.1029/95JA03673>
- Luhmann, J. G., Dong, D., Ma, Y., Curry, S. M., Mitchell, D., Espley, J., et al. (2015). Implications of MAVEN Mars near-wake measurements and models. *Geophysical Research Letters*, 42, 9087–9094. <https://doi.org/10.1002/2015GL066122>
- Lundin, R. (2011). Ion acceleration and outflow from Mars and Venus: An Overview. *Space Science Reviews*, 162, 309–334. <https://doi.org/10.1007/s11214-011-9811-y>
- Ma, Y., Nagy, A. F., Sokolov, I. V., & Hansen, K. C. (2004). Three-dimensional, multispecies, high spatial resolution MHD studies of the solar-wind interaction with Mars. *Journal of Geophysical Research*, 109. <https://doi.org/10.1029/2003JA010367>
- Ma, Y., Russell, C. T., Toth, G., Chen, Y., Nagy, A. F., Harada, Y., et al. (2018). Reconnection in the Martian Magnetotail: Hall-MHD with embedded particle-in-cell simulations. *Journal of Geophysical Research: Space Physics*, 123, 3742–3763. <https://doi.org/10.1029/2017JA024729>
- Ma, Y. J., Russell, C. T., Fang, X., Dong, Y., Nagy, A. F., Toth, G., et al. (2015). MHD model results of solar wind interaction with Mars and comparison with MAVEN plasma observations. *Geophysical Research Letters*, 42, 9113–9120. <https://doi.org/10.1002/2015GL065218>
- Marquette, M. L., Lillis, R. J., Halekas, J. S., Luhmann, J. L., Gruesbeck, J. R., & Espley, J. R. (2018). Autocorrelation study of solar wind plasma and IMF properties as measured by the MAVEN spacecraft. *Journal of Geophysical Research: Space Physics*, 123, 2493–2512. <https://doi.org/10.1002/2018JA025209>
- Mitchell, D. L., Lin, R. P., Mazelle, C., Rème, H., Cloutier, P. A., Connerney, J. E. P., et al. (2001). Probing Mars' crustal magnetic field and ionosphere with the MGS Electron Reflectometer. *Journal of Geophysical Research*, 106, 23419–23427. <https://doi.org/10.1029/2000JE001435>
- Modolo, R., Chanteur, G. M., & Dubinin, E. (2012). Dynamic Martian magnetosphere: Transient twist induced by a rotation of the IMF. *Geophysical Research Letters*, 39. <https://doi.org/10.1029/2011GL049895>
- Owen, C. J., Slavin, J. A., Richardson, I. G., Murphy, N., & Hynds, R. J. (1995). Average motion, structure and orientation of the distant magnetotail determined from remote sensing of the edge of the plasma sheet boundary layer with E > 35 keV ions. *Journal of Geophysical Research*, 100, 185. <https://doi.org/10.1029/94JA02417>
- Parker, E. N. (1958). *Dynamics of the interplanetary gas and magnetic fields*. Astrophys Journal. <https://doi.org/10.1086/146579>
- Pitknen, T., Kullen, A., Cai, L., Park, J.-S., Vanhamäki, H., Hamrin, M., et al. (2021). Asymmetry in the Earth's magnetotail neutral sheet rotation due to IMF by sign? *Geoscience Letters*, 8. <https://doi.org/10.1186/s40562-020-00171-7>
- Ramstad, R., Brain, D. A., Dong, Y., Espley, J. R., Halekas, J. S., & Jakosky, B. (2020). The global current systems of the Martian induced magnetosphere. *Nature Astronomy*. <https://doi.org/10.1038/s41550-020-1099-y>
- Romanelli, N., Bertucci, C., Gomez, D., & Mazelle, C. (2015). Dependence of the location of the Martian magnetic lobes on the interplanetary magnetic field direction: Observations from Mars Global Surveyor. *Journal of Geophysical Research: Space Physics*, 120, 7737–7747. <https://doi.org/10.1002/2015JA021359>
- Romanelli, N., DiBraccio, G., Halekas, J., Dubinin, E., Gruesbeck, J., Espley, J., et al. (2020). Variability of the solar wind flow asymmetry in the Martian magnetosheath observed by MAVEN. *Geophysical Research Letters*, 47. <https://doi.org/10.1029/2020GL090793>

- Romanelli, N., Modolo, R., Leblanc, F., Chaufray, J.-Y., Hess, S., Brain, D., et al. (2018). Effects of the crustal magnetic fields and changes in the IMF orientation on the magnetosphere of Mars: MAVEN observations and Lathys results. *Journal of Geophysical Research: Space Physics*, *123*, 5315–5333. <https://doi.org/10.1029/2017JA025155>
- Ruhunusiri, S., Halekas, J. S., Espley, J. R., Eparvier, F. G., Brain, D. A., Mazelle, C., et al. (2018). An artificial neural network for inferring solar wind proxies at Mars. *Geophysical Research Letters*, *45*. <https://doi.org/10.1029/2018GL079282>
- Sibeck, D. G., Siscoe, G. L., Slavin, J. A., Smith, E. J., Tsurutani, B. T., & Lepping, R. P. (1985). The distant magnetotail's response to a strong interplanetary magnetic field By: Twisting, flattening, and field line bending. *Journal of Geophysical Research*, *90*, 4011. <https://doi.org/10.1029/JA090iA05p04011>
- Sonnerup, B. U. Ö. (1974). Magnetopause reconnection rate. *Journal of Geophysical Research*. <https://doi.org/10.1029/JA079i010p01546>
- Tenfjord, P., Østgaard, N., Snekvik, K., Laundal, K. M., Reistad, J. P., Haaland, S., & Milan, S. E. (2015). How the IMF By induces a By component in the closed magnetosphere and how it leads to asymmetric currents and convection patterns in the two hemispheres. *Journal of Geophysical Research: Space Physics*, *120*, 9368–9384. <https://doi.org/10.1002/2015JA021579>
- Ulusen, D., Luhmann, J. G., Ma, Y., & Brain, D. A. (2016). Solar control of the Martian magnetic topology: Implications from model-data comparisons. *Planetary and Space Science*, *128*, 1–13. <https://doi.org/10.1016/j.pss.2016.01.007>
- Vignes, D., Mazelle, C., Rme, H., Acuña, M. H., Connerney, J. E. P., Lin, R. P., et al. (2000). The solar wind interaction with Mars: Locations and shapes of the bow shock and the magnetic pile-up boundary from the observations of the MAG/ER experiment on-board Mars global surveyor. *Geophysical Research Letters*, *27*, 49–52. <https://doi.org/10.1029/1999GL010703>
- Weber, T., Brain, D., Mitchell, D., Xu, S., Connerney, J., & Halekas, J. (2017). Characterization of low-altitude nightside Martian magnetic topology using electron pitch angle distributions. *Journal of Geophysical Research: Space Physics*, *122*, 9777–9789. <https://doi.org/10.1002/2017JA024491>
- Weber, T., Brain, D., Mitchell, D., Xu, S., Espley, J., Halekas, J., et al. (2019). The influence of solar wind pressure on Martian crustal magnetic field topology. *Geophysical Research Letters*, *46*, 2347–2354. <https://doi.org/10.1029/2019GL081913>
- Weber, T., Brain, D., Xu, S., Mitchell, D., Espley, J., Halekas, J., et al. (2020). The influence of interplanetary magnetic field direction on Martian crustal magnetic field topology. *Geophysical Research Letters*, *47*. <https://doi.org/10.1029/2020GL087757>
- Xiao, S., Zhang, T., Ge, Y., Wang, G., Baumjohann, W., & Nakamura, R. (2016). A statistical study on the shape and position of the magnetotail neutral sheet. *Annales de Geophysique*, *34*, 303–311. <https://doi.org/10.5194/angeo-34-303-2016>
- Xu, S., Mitchell, D., Liemohn, M., Dong, C., Bougher, S., Fillingim, M., et al. (2016). Deep nightside photoelectron observations by MAVEN SWEA: Implications for Martian northern hemispheric magnetic topology and nightside ionosphere source. *Geophysical Research Letters*, *43*, 8876–8884. <https://doi.org/10.1002/2016GL070527>
- Xu, S., Mitchell, D., Liemohn, M., Fang, X., Ma, Y., Luhmann, J., et al. (2017). Martian low-altitude magnetic topology deduced from MAVEN/SWEA observations. *Journal of Geophysical Research: Space Physics*, *122*, 1831–1852. <https://doi.org/10.1002/2016JA023467>
- Xu, S., Mitchell, D., Luhmann, J., Ma, Y., Fang, X., Harada, Y., et al. (2017). High-altitude closed magnetic loops at Mars observed by MAVEN. *Geophysical Research Letters*, *44*, 229–11. <https://doi.org/10.1002/2017GL075831>
- Xu, S., Mitchell, D. L., Weber, T., Brain, D. A., Luhmann, J. G., Dong, C., et al. (2020). Characterizing Mars's magnetotail topology with respect to the upstream interplanetary magnetic fields. *Journal of Geophysical Research: Space Physics*, *125*. <https://doi.org/10.1029/2019JA027755>
- Xu, S., Weber, T., Mitchell, D. L., Brain, D. A., Mazelle, C., DiBraccio, G. A., & Espley, J. (2019). A technique to infer magnetic topology at Mars and its application to the terminator region. *Journal of Geophysical Research: Space Physics*, *124*, 1823–1842. <https://doi.org/10.1029/2018JA026366>
- Yeroshenko, Y., Riedler, W., Schwingenschuh, K., Luhmann, J. G., Ong, M., & Russell, C. T. (1990). The Magnetotail of Mars: Phobos Observations. *Geophysical Research Letters*. <https://doi.org/10.1029/GL017i006p00885>